Mesoscale Simulations of Fluid-Fluid Interfaces

T. Krüger, S. Frijters, F. Günther, B. Kaoui, and Jens Harting

Abstract Fluid-fluid interfaces appear in numerous systems of academic and industrial interest. Their dynamics is difficult to track since they are usually deformable and of not a priori known shape. Computer simulations pose an attractive way to gain insight into the physics of interfaces. In this report we restrict ourselves to two classes of interfaces and their simulation by means of numerical schemes coupled to the lattice Boltzmann method as a solver for the hydrodynamics of the problem. These are the immersed boundary method for the simulation of vesicles and capsules and the Shan-Chen pseudopotential approach for multi-component fluids in combination with a molecular dynamics algorithm for the simulation of nanoparticle stabilized emulsions. The advantage of these algorithms is their inherent locality allowing to develop highly scalable codes which can be used to harness the computational power of the currently largest available supercomputers.

T. Krüger
Department of Applied Physics, Eindhoven University of Technology, Den Dolech 2, 5600MB Eindhoven, The Netherlands

School of Engineering, Institute for Materials and Processes, University of Edinburgh, Mayfield Road, Edinburgh EH9 3JL, Scotland, UK

S. Frijters • F. Günther
Department of Applied Physics, Eindhoven University of Technology, Den Dolech 2, 5600MB Eindhoven, The Netherlands

B. Kaoui
Department of Applied Physics, Eindhoven University of Technology, Den Dolech 2, 5600MB Eindhoven, The Netherlands

Theoretical Physics I, University of Bayreuth, Universitätsstrasse 30, 95447 Bayreuth, Germany

J. Harting (✉)
Department of Applied Physics, Eindhoven University of Technology, Den Dolech 2, 5600MB Eindhoven, The Netherlands

Institute for Computational Physics, University of Stuttgart, Allmandring 3, 70569 Stuttgart, Germany
e-mail: jens@icp.uni-stuttgart.de

W.E. Nagel et al. (eds.), *High Performance Computing in Science and Engineering '14*, DOI 10.1007/978-3-319-10810-0_36

1 Introduction

Interfaces are ubiquitous in soft matter systems and appear in various shapes and sizes. Prominent examples are capsules and all kinds of biological cells [1, 2]. In these cases, the interface is an additional material whose constitutive behavior has to be specified. Understanding the dynamics of membranes is important for disease detection by measuring mechanical properties of living cell membranes [3], targeted drug delivery [4], and predicting the viscosity of biofluids, such as blood [5]. Typical applications are lab-on-chip devices for particle identification and separation [6].

Other classes of fluid-fluid interfaces can be found in emulsions (liquid drops suspended in another liquid), foams (gas bubbles separated by thin liquid films), and liquid aerosols (liquid drops in gas) where at least two immiscible fluid phases are mixed. The interface is then defined by the common boundaries of the phases. Emulsions are of central importance for food processing (e.g., milk, salad dressings), pharmaceutics (e.g., lotions, vaccines, disinfection), and enhanced oil recovery.

Emulsions and foams are usually unstable. Drops and bubbles tend to coalesce gradually, which reduces the interfacial free energy. The traditional approach for the stabilization of emulsions is to add surfactants [7]. Surfactants are amphiphilic molecules for which it is energetically favorable to accumulate at the interface, which in turn leads to a decrease of surface tension and prevents demixing. Alternatively, emulsions can be stabilized by using colloidal particles: these particles also accumulate at the interface where they replace segments of fluid-fluid interface by fluid-particle interfaces and thus lower the interfacial free energy. However, the physical mechanism is different from that of stabilization by surfactants, and the surface tension is unchanged by the nanoparticles [8, 9]. For nanoparticle-stabilized emulsions, one distinguishes between so-called "Pickering emulsions" [10, 11] and "bijels" (bicontinuous interfacially jammed emulsion gels) [12, 13]. The former is an emulsion of discrete droplets in a continuous liquid. In the latter, both phases are continuously distributed.

Fluid-fluid interface problems are hard to solve analytically since the interface is usually deformable and its shape not known a priori. Therefore, the interface dynamics is fully coupled to that of the ambient phases. Analytical solutions are only available for academic cases. These circumstances call for numerical methods and computer simulations which can also provide access to observables not traceable in experiments such as local interface curvature or fluid and interface stresses. Therefore, computer simulations can be used to complement experiments.

In this report, we focus on capsules and emulsions in systems with dimensions comparable to the lateral extension of the interfaces. At this scale, fluid dynamics is dominated by effects due to viscosity, surface tension or elasticity, and inertia. Gravity is usually not relevant in microfluidics because the capillary length for water droplets in air is typically of the order of a few millimeters. The relative strength of the three major contributions (viscosity, surface tension, inertia) can be described by dimensionless parameters, such as the capillary number (Ca, viscous stress vs.

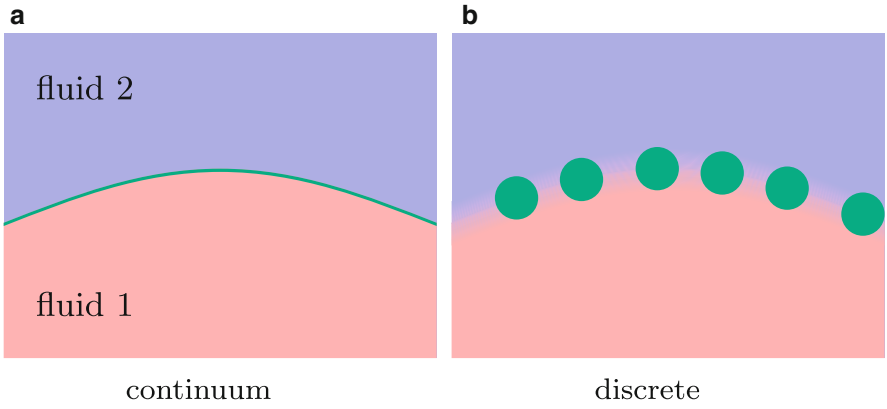

Fig. 1 Coarse-graining levels for a fluid-fluid interface (fluids 1 and 2). (**a**) the interface (*green line*) is explicitly tracked in a Lagrangian manner, and the interface properties have to be provided in form of a constitutive law. There is no direct interaction between the fluid species. The substructure of the interface is not known (continuum picture). (b) nanoparticles (*green*) are explicitly resolved (discrete picture). Their individual motions are tracked, and their geometrical and interaction properties have to be specified (e.g., shape, contact angles). The interaction of the fluid species has to be defined as well. For (**b**), the choice of the mutual interactions leads to an emergent macroscopic interface behaviour (From [1])

surface tension or elasticity), the Reynolds number (Re, inertial vs. viscous stresses), or the Weber number (We, inertial stress vs. surface tension).

In the current report, the fluid phases are treated as Newtonian fluids simulated by the lattice Boltzmann method (detailed in Sect. 2.1). Depending on the physical conditions and the desired level of coarse-graining, it may be sufficient to treat the interface as an effective two-dimensional material obeying a well-defined constitutive law or it may be necessary to resolve the substructure of the interface (cf. Fig. 1). Following Ref. [1], we consider two cases. In the continuum description for capsule membranes, the immersed boundary method is coupled to the single-component lattice Boltzmann (LB) method (Sect. 2.2). The LB Shan-Chen multi-component model is the basis for the other case where explicitly resolved solid nanoparticles interact with the fluid phases (Sect. 2.3). In Sect. 3, we present several examples (separation of red blood cells and platelets on the one hand and particle stabilized interfaces on the other hand). Finally, we conclude in section “Conclusions”.

2 Numerical Approaches

The physical problem consists in capturing the dynamics of an interface separating distinct fluids. In the simplest situation, there are two different fluids separated by an interface. Mathematically, this corresponds to two domains separated by a free-moving boundary. There are two classes of numerical approaches to track the

motion of an interface: (i) either *front tracking* (e.g., the boundary integral method or the immersed boundary method) in which the motion of marker points attached to the interface is tracked, or (ii) *front capturing* (e.g., the phase field method or level set methods) where a scalar field is used as an order parameter, indicating the composition of the fluid at a given point. In both approaches, the momentum of the incompressible Newtonian fluids obeys the Navier-Stokes (NS) equations.

2.1 Lattice-Boltzmann Method

Instead of solving the NS equations directly, we use a mesoscopic approach: the *lattice Boltzmann method* (LBM). The LBM has gained popularity among scientists and engineers because of its relatively straightforward implementation compared to other approaches such as the finite element method (for reviews, see [14, 15]). In the LBM, the fluid is considered as a cluster of pseudo-particles that move on a lattice under the action of external forces. To each pseudo-particle is associated a distribution function f_i, the main quantity in the LBM. It gives the probability to find a pseudo-particle at a position $\mathbf{r}$ with a velocity in direction $\mathbf{e}_i$. In the LBM, both the position and velocity spaces are discretised: Δx is the grid spacing, and $\mathbf{e}_i$ are the discretised velocity directions. The time evolution of f_i is governed by the so-called lattice Boltzmann equation,

$$f_i(\mathbf{r} + \mathbf{e}_i \Delta t, t + \Delta t) - f_i(\mathbf{r}, t) = \Omega_i, \tag{1}$$

where Δt is the discrete time step. We approximate the collision operator Ω_i by the Bhatnagar-Gross-Krook (BGK) operator, $\Omega_i = -(f_i - f_i^{\mathrm{eq}})/\tau$, which describes the relaxation of f_i towards its local equilibrium, f_i^{eq}, on a time scale τ. The relaxation time is related to the macroscopic dynamical viscosity η via $\eta = \rho c_{\mathrm{s}}^2 \frac{\Delta x^2}{\Delta t} \left(\tau - \frac{1}{2}\right)$, where $c_{\mathrm{s}} = 1/\sqrt{3}$ is the lattice speed of sound. The equilibrium distribution is given by a truncated Maxwell-Boltzmann distribution. The hydrodynamical macroscopic quantities are computed using the first and the second moments of f_i.

The LBM can also handle multi-phase and multi-component fluids and a number of corresponding extensions of the method have been published in the past [16–19]. In the Shan-Chen multi-component model [16], a system containing N miscible or immiscible fluids (with index σ) are described by N sets of distribution functions $f_{\sigma,i}$, one for each species. As a consequence, N lattice Boltzmann equations with relaxation times τ_σ have to be considered. The interaction between the fluid species is mediated via a local force density. The Shan-Chen model belongs to the class of front capturing methods. It is suitable to track interfaces for which the topology evolves in time, for example, the breakup of a droplet.

2.2 Continuum Interface Model

In this section, we present the *immersed boundary method* (IBM) as a front tracking approach [20]. Such methods are mostly employed when the interface is formed by an additional continuous material whose constitutive behaviour (e.g., elasticity, viscosity) is assumed to be known. Examples are capsules, vesicles, or biological cells.

Within the IBM, the interface is considered sharp (zero thickness) and is represented by a cluster of marker points (nodes) which constitute a moving Lagrangian mesh (cf. Fig. 2a). This mesh is immersed in a fixed Eulerian lattice representing the fluid. To consider correct dynamics, a bi-directional coupling of the lattice fluid and the moving Lagrangian mesh has to be taken into account. On the one hand, the interface is modelled as an impermeable structure obeying the no-slip condition at its surface. It is assumed that the flow field is continuous across the interface and that the interface is massless. Therefore, the interface is moving along with the ambient fluid velocity. On the other hand, a deformation of the interface generally leads to stresses reacting back onto the fluid via local forces. The stresses depend on the chosen constitutive behaviour of the interface and are not predicted within the IBM itself. The two-way coupling is accomplished in two main steps (as detailed in [20] and [21]): (i) velocity interpolation and Lagrangian node advection and (ii) force spreading (reaction).

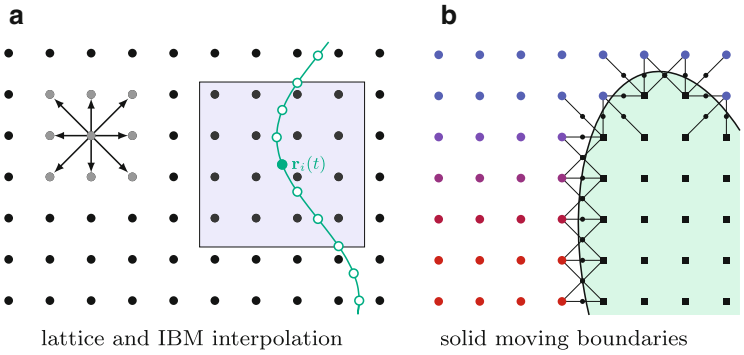

Fig. 2 Two-dimensional illustrations of the lattice Boltzmann propagation, immersed boundary interpolation, and bounce-back. (**a**) During propagation, the populations f_i move to their next neighbors (*gray lattice sites and arrows*). Within the immersed boundary method, an interface node (here: node i at position $\mathbf{r}_i(t)$) is coupled to the single-component lattice fluid. The range of the interpolation stencil (here: 4×4) is denoted by the square region. All lattice sites within this region have to be considered during velocity interpolation and force spreading. (**b**) An ellipsoidal nanoparticle is located at a fluid-fluid interface. One fluid component is indicated by *red*, the other by *blue circles*. The colour gradient illustrates the interface region. *Squares* denote lattice sites inside the particle. Populations are bounced back at points (shown as *small circles*) located half-way between neighbouring fluid and particle sites. This gives rise to an effective staircase description of the particle shape (From [1])

2.3 Discrete Interface Model

If there is no clear scale separation between immersed particles and the lateral interface extension, it may be necessary to model the particles explicitly. Here, we consider an ensemble of particles with well-defined wetting behaviour. There are several approaches to simulate a system of two immiscible fluids and particles. One example which has recently been applied by several groups is Molecular Dynamics (MD) coupled to the LBM [9, 12, 22–27]. The advantage of this combination is the possibility to resolve the particles as well as both fluids in such a way that all relevant hydrodynamical properties are included. The particles are generally assumed to be rigid and can have arbitrary shapes, where we restrict ourselves to spheres and ellipsoids.

For the fluid-particle coupling, the particles are discretised on the lattice: sites which are occupied by a particle are marked as solid. Following the approach proposed by Ladd [28], populations propagating from fluid to particle sites are bounced back in the direction they came from (cf. Fig. 2b). In this process, the populations receive additional momentum due to the motion of the particles. In the context of the Shan-Chen multi-component algorithm coupled to the particle solver, the outermost sites covered by a particle are filled with a virtual fluid corresponding to a suitable average of the surrounding unoccupied sites. This approach provides accurate dynamics of the two-component fluid near the particle surface. The wetting properties of the particle surface can be controlled by shifting the local density difference of both fluid species by a given amount $\Delta\rho$. Occasionally, when the particles move, lattice sites change from particle to fluid state, which has to be treated properly [9, 22].

3 Case Studies

The simulations presented in this report have been peformed using our simulation code *LB3D* which combines a ternary amphiphilic multicomponent lattice Boltzmann solver with a molecular dynamics module for suspended solid particles and an immersed boundary method module for deformable objects. The code has shown excellent performance and scaling behaviour in the past and was the workhorse for several previous projects on HLRS and SSC Karlsruhe HPC installations. As such, we refer the reader to the according references for technical details [1, 7, 9, 22–25, 29, 30]. In general, the simulations presented in the following case studies can be seen as building blocks for large scale simulations containing many particles, cells, or droplets. Those simulations are by definition very costly since the 3D dynamic solution of the lattice Boltzmann equation together with the interface dynamics requires generally large systems of at least 256^3 or 512^3 lattice nodes and has to run for several million timesteps. A simulation of such kind easily requires several days on several thousand cores on state of the art Tier-0 HPC resources.

3.1 Flow-Induced Separation of Red Blood Cells and Platelets

In this section, we show three-dimensional simulations of the separation of blood components as an example for the immersed-boundary-lattice-Boltzmann method (Sect. 2.2).

Efficient separation of biological cells plays a major role in present-day medical applications, for example, the detection of diseased cells or the enrichment of rare cells. While active cell sorting relies on external forces acting on tagged particles, the idea of passive sorting is to take advantage of hydrodynamic effects in combination with the cells' membrane (interface) properties. It is known that deformable and rigid particles behave differently when exposed to external flow fields. For example, in Stokes flow (Re $=$ 0), deformable capsules show a strong tendency to migrate towards the centreline of a pressure-gradient driven channel flow. Therefore, it has been proposed to use the particle deformability as intrinsic marker to separate rigid and deformable particles in specifically designed microfluidic devices. We show that the separation of red blood cells (RBCs) and platelets, which has been shown recently via experiments [31], can be simulated by means of the LBM and immersed boundary method.

The RBCs and platelets are modelled as closed two-dimensional membranes with identical fluids in the interior and exterior regions. In the present approach, a finite element method is used to compute the local surface shear deformation and area dilatation and the resulting forces [32–34]. 40 RBCs and 30 platelets are randomly distributed in the bottom 30 % of a channel segment with $50\times50\times50\,\mu\text{m}^3$ volume, cf. Fig. 3. The platelets can be considered as rigid ellipsoidal particles. The large RBC and platelet diameters are 16 and 5.5 lattice constants, respectively. The channel is bounded by two parallel walls and is periodic in the other two directions. A force f in rightward direction is used to drive the flow, resulting in a Poiseuille-

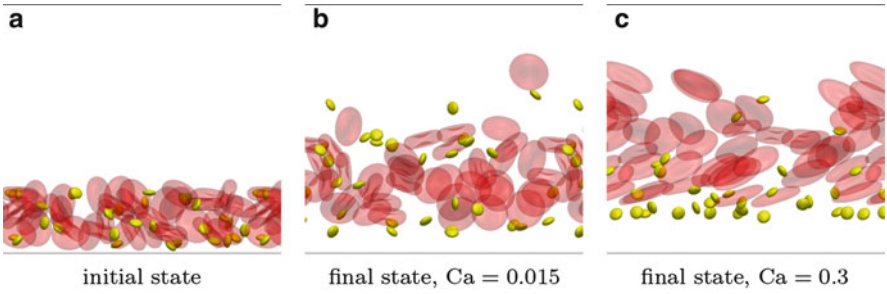

Fig. 3 Simulation snapshots of the separation of red blood cells (RBCs) and platelets. (**a**) Initially, the random suspension is located in the bottom 30 % of the channel (50 μm diameter, denoted by two black lines). RBCs (*red*) are shown with reduced opacity to reveal the platelet positions (*yellow*). Panels (**b**) and (**c**) show the lateral distribution of the cells after they have been moving downstream (rightwards) by about 20 mm on average. For rigid and tumbling RBCs, lateral separation of RBCs and platelets is not pronounced (**b**). The separation is more efficient when the RBCs are strongly deformable and are tank-treading in the vicinity of the walls (**c**) (From [1])

like velocity profile. The RBC membrane (interface) is characterised by the capillary number $\mathrm{Ca} = \eta\dot{\gamma}r/\kappa_s$. Here, $\dot{\gamma}$ is the average shear rate, $r = 4\,\mu\mathrm{m}$ is the large RBC radius and κ_s is its shear elasticity which is about $5\,\mu\mathrm{N\,m^{-1}}$ for healthy RBCs. Two simulations have been run, one with the normal elasticity, leading to $\mathrm{Ca} = 0.3$ for the selected viscosity and driving force. In the other case, the RBC shear modulus has been increased by a factor of 20, and the capillary number was 0.015. This situation is typical for diseased RBCs (e.g., due to malaria or sickle cell anaemia).

The initial simulation states are shown in Fig. 3a, while the panels (b) and (c) show the state after about 20 mm downstream motion for different capillary numbers. It can be seen that RBCs and platelets can be efficiently separated when the RBCs are sufficiently deformable (Fig. 3c). The platelets marginate into the gap forming between the bottom wall and the RBC bulk. Contrarily, for the rigid RBCs, separation is visible but not pronounced (Fig. 3b). Additionally, the bulk of the RBCs moves faster towards the centreplane when the particles are more deformable, i.e., when Ca is larger. For $\mathrm{Ca} = 0.30$, RBCs near the wall are observed to tank-tread; for $\mathrm{Ca} = 0.015$, all are tumbling.

3.2 Ellipsoidal and Spherical Particles at Fluid Interfaces

We now consider the effect of massive nanoparticles adsorped to a fluid-fluid interface as an example of the coupled lattice Boltzmann-molecular dynamics method explained in Sect. 2.3. The first example shows the ordering of ellipsoidal particles at the interface of a spherical fluid droplet and compares it with the corresponding results of particles at a flat interface. This is followed by a case study highlighting how the presence of spherical nanoparticles affects the properties of a droplet in shear flow.

Particles adsorbed at a fluid-fluid interface can stabilise emulsions of immiscible fluids (e.g., Pickering emulsions where droplets of one fluid are immersed in another fluid and are stabilised by colloidal particles) [22–24]. These colloids are not necessarily spherical, e.g. clay particles, which have a flat shape. A simple approximation of such a particle shape is an ellipsoid. In this section, the behaviour of an ensemble of elongated ellipsoidal particles with aspect ratio $m = 2$ at a single droplet interface is discussed [35]. The results are compared to the corresponding case of a flat interface. The initial particle orientation is such that the long axis is orthogonal to the local interface (cf. Fig. 4a). As discussed in [23,24], for the case of a single prolate ellipsoidal particle at a flat interface, the equilibrium configuration is a particle orientation parallel to the interface. The simulations discussed in this section have been performed for coverage fractions $\chi = 0.153$ and $\chi = 0.305$.

Figure 4a, b show the particle laden droplet at the beginning of the simulation where all particles are perpendicular to the interface for both values of χ. For the case of $\chi = 0.305$, the particles are comparably close to each other so that capillary interactions lead to the clustering motion of particles. In Fig. 4c, at the end of the simulation, the particles have completed a rotation towards the interface

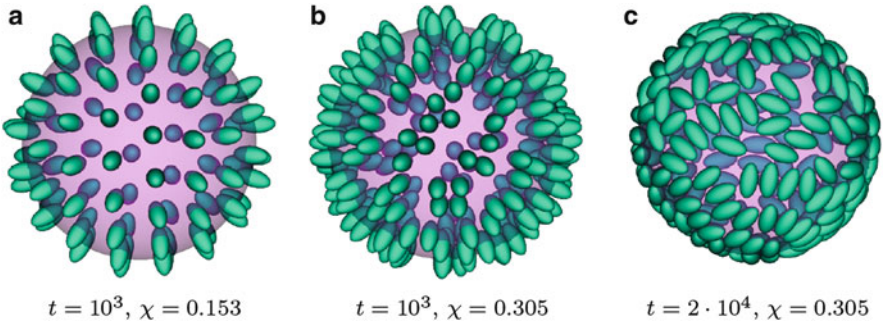

Fig. 4 Snapshots of a particle-laden droplet for different times (in time steps) and coverage fractions χ. One observes a higher global spatial order for the more dilute system in (**a**) as compared to the denser case in (**b**) (From [1])

and stabilise the largest interfacial area possible. However, their local dynamics and temporal re-ordering is a continuous interplay between capillary interactions, hydrodynamic waves due to interface deformations and particle collisions.

Inspired from liquid crystal analysis, we use the uniaxial order parameter S to characterise the orientational ordering of anisotropic particles. Figure 5a shows the time evolution of the order parameter S for particles at a droplet interface for $\chi = 0.153$ and $\chi = 0.305$ and the corresponding cases for particles at a flat interface. Initially, the order parameter assumes the value $S_\perp = 1$ which corresponds to perfect alignment perpendicularly to the interface. In the case of flat interfaces, the order parameter reaches the final value of $S \approx S_\parallel = -0.5$. This corresponds to the state where all particles are aligned with the interface plane. For particle laden droplets (cf. Fig. 4c), a value of $S \approx -0.4 > S_\parallel$ is found, which indicates that the particles are not entirely aligned with the interface. Furthermore, S fluctuates in time. One possible reason for this deviation of S from $S_\parallel$ is that the droplet does not have the exact spherical shape which is assumed for the calculation of S. The fluctuation of S can be explained by distortions of the droplet shape due to the dynamics of the particle rotations. Another difference between the curved and the flat interface is the time scale for the particle flip.

To measure the spatial short range ordering of the particles, we define a pair correlation function $g(r)$ In Fig. 5b, the time dependence of $g(r)$ is shown for a spherical interface and $\chi = 0.305$. One notices that all maxima decrease in time. This means that the local ordering decreases, particularly in the first 10^4 time steps. Afterwards, $g(r)$ changes only slightly. Figure 5c compares $g(r)$ for $\chi = 0.153$ and $\chi = 0.305$ after 10^3 time steps and can be used to explain the differences of the snapshots in Fig. 4a, b: the order is higher for a smaller concentration χ. In the case of $\chi = 0.305$, the ellipsoids are attracted by capillary forces leading to a clustering of particles. This causes disorder, which manifests itself in smaller peak amplitudes of $g(r)$.

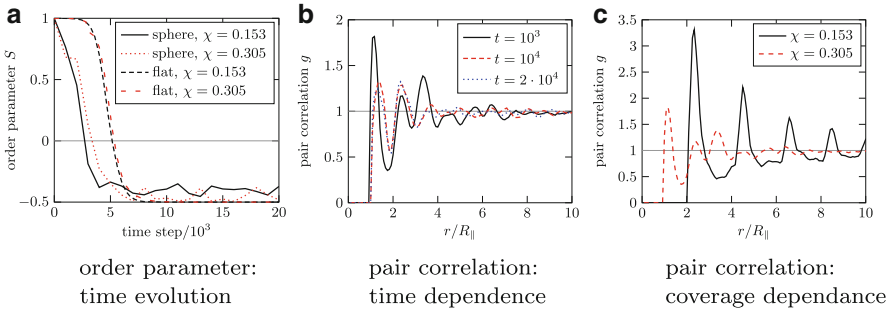

Fig. 5 (**a**) Time evolution of the uniaxial order parameter S: the order decreases faster for the case of a sphere while the coverage fraction does not play an appreciable role. (**b**) The time dependence of the pair correlation function $g(r)$ for particles adsorbed at a spherical interface ($\chi = 0.305$) is shown for different times. (**c**) Pair correlation function for the spherical interface after 10^3 time steps for different values of χ corresponding to Fig. 4a, b (From [1])

To summarize, the particle coverage χ has a marginal influence on the duration of the flipping towards the interface. However, the particles rotate faster when the interface is spherical. For increasing χ, the spatial particle ordering is reduced since the average particle distance is sufficiently small to allow for attractive capillary forces which in turn cause particle clustering.

In many industrial applications, the particle-covered droplets as discussed in the previous example are not stationary or in equilibrium, but are instead subjected to external stresses or forces. The properties of the individual droplets are then of interest as their behaviour dictates that of, for example, an emulsion formed of these droplets. In this example, we consider monodisperse neutrally wetting spherical particles. The particles are adsorped to the droplet interface which is initially spherical. External shear is realised by using Lees-Edwards boundary conditions [36]. As this shear is applied to the system, the droplet will start to deform. To quantify this deformation, for small to moderate shear rates $\dot{\gamma}$, a dimensionless deformation parameter is used: $D = (L - B)/(L + B)$ where L is the length and B is the breadth of the droplet. This parameter will be zero for a sphere and tend to unity for a very strongly elongated droplet. As the droplet loses its spherical symmetry, it will also start to exhibit an angle of its long axis with respect to the shear flow: the inclination angle θ_d.

Increasing the shear rate a droplet is subjected to will generally increase its deformation, as well as reduce its inclination angle from an initial angle of 45°: the droplet is elongated and aligns with the shear flow. However, this is only valid as long as inertia can be neglected. When inertial forces are comparable to or stronger than viscous forces, the inclination angle can first increase beyond 45°, before its eventual reduction. We now discuss the effect of increasing the particle coverage fraction χ at constant shear rates $\dot{\gamma}$. Representative snapshots of the droplets for various χ and fixed $\dot{\gamma} = 0.47 \cdot 10^{-3}$ are presented in Fig. 6a–c. The particles are not homogeneously distributed over the droplet surface when shear is applied, due to

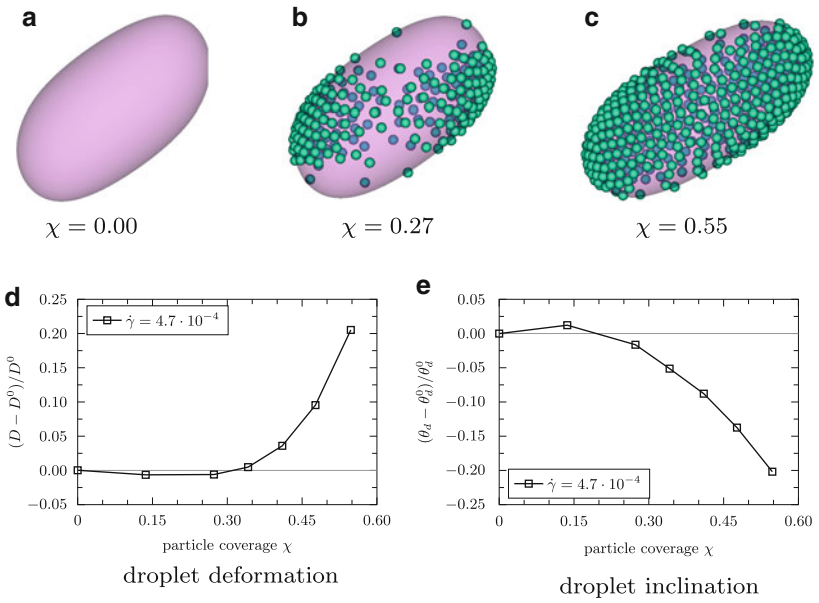

Fig. 6 Effect of adding monodisperse and neutrally wetting spherical nanoparticles to the interface of a droplet in shear flow. Representative snapshots of deformed particle-covered droplets are shown for $\dot{\gamma} = 4.7 \cdot 10^{-4}$ and (**a**) $\chi = 0$, (**b**) $\chi = 0.27$, and (**c**) $\chi = 0.55$ ([9], reproduced with permission of the Royal Society of Chemistry). The relative deformation of the droplet increases strongly for high coverage fraction, as shown in (**d**). In turn, the relative inclination angle decreases, indicating a better alignment with the shear flow, as shown in (**e**) (From [1])

an interplay between local curvature and shear velocities: high curvatures and low velocities are energetically favoured.

Figure 6d shows the change in deformation of the droplet as the particle coverage is increased. The deformation has been rescaled as $D^* = (D - D^0)/D^0$, where $D^0 \equiv D(\chi = 0)$. Due to a large decrease in free energy granted by the presence of particles at the interface, they are irreversibly adsorbed. When shear is applied, the particles are affected by this, and they start to move over the droplet surface, but cannot be swept away. As can be seen from the figure, high particle coverage fractions lead to a large increase in deformation of the droplet. The inertia of the particles plays a critical role here. The particles have to reverse direction to stay attached to the droplet, and massive particles strongly resist this change in velocity. This causes the interface to be dragged by the particles, increasing elongation from the tips. Figure 6e demonstrates the effect of particle coverage on the inclination angle of the droplet. Similar to the rescaling performed on the deformation, the inclination angle has been rescaled as $\theta_d^* = (\theta_d - \theta_d^0)/\theta_d^0$, where $\theta_d^0 \equiv \theta(\chi = 0)$. The inertial effects described above also cause the inclination angle to strongly decrease for large χ.

4 Conclusions

We presented a few of our recent applications of lattice Boltzmann based simulation methods to fluid-fluid interface problems: the immersed boundary method offers a flexible and simple approach to model deformable particles immersed in suspending fluids. As it is a front-tracking method, the interface configuration is directly known, which simplifies the force evaluation based on the interface deformation. Another advantage is that the constitutive properties of the interface can be controlled directly without tuning additional simulation parameters, and there is no need to remesh the fluid domain. Therefore, an implementation as ours can be used to simulate tens of thousands suspended deformable particles flowing in complex geometries on current supercomputers.

When the multi-component lattice Boltzmann method is coupled to a molecular dynamics algorithm for the description of suspended (colloidal) particles, particle-laden interfaces can be studied at a level where not only hydrodynamics, but also individual particles and their interactions are resolved. At the same time, efficient scaling to allow larger domains to be simulated is still provided due to the locality of the algorithm. While this method has been proven to be particularly suitable to study particle stabilised emulsions, one of its drawbacks is the diffuse interface between fluids in the Shan-Chen LBM. The particles have to be substantially larger than these diffuse interfaces in order to be able to stabilise them. Thus, even comparably simple applications as the ones provided in this report require large lattices and therefore access to supercomputing resources. However, the excellent performance and scaling behviour of the simulation method and our implementation *LB3D* has been demonstrated on several available supercomputing platforms including Hermit.

Acknowledgements Financial support is greatly acknowledged from NWO/STW (Vidi grant 10787 of J. Harting) and FOM/Shell IPP (09iPOG14 – "Detection and guidance of nanoparticles for enhanced oil recovery"). We thank the Gauss Center for Supercomputing and HLRS Stuttgart for the allocation of computating time on Hermit.

References

1. Krüger, T., Frijters, S., Günther, F., Kaoui, B., Harting, J.: Numerical simulations of complex fluid-fluid interface dynamics. Eur. Phys. J. Spec. Topics **222**, 177 (2013)
2. Pozrikidis, C. (ed.) Modeling and Simulation of Capsules and Biological Cells. Chapman & Hall/CRC Mathematical Biology and Medicine Series. Chapman & Hall/CRC, Boca Raton (2003)
3. Suresh, S., Spatz, J., Mills, J., Micoulet, A., Dao, M., Lim, C., Beil, M., Seufferlein, M.: Connections between single-cell biomechanics and human disease states: gastrointestinal cancer and malaria. Acta Biomater. **1**, 15–30 (2005)
4. Battaglia, L., Gallarate, M.: Lipid nanoparticles: state of the art, new preparation methods and challenges in drug delivery. Expert Opin. Drug Deliv. **9**(5), 497–508 (2012)

5. Fedosov, D., Pan, W., Caswell, B., Gompper, G., Karniadakis, G.: Predicting human blood viscosity in silico. Proc. Natl. Acad. Sci. **108**(29), 11772 (2011)
6. Hou, H., Bhagat, A., Chong, A., Mao, P., Tan, K., Han, J., Lim, C.: Deformability based cell margination—A simple microfluidic design for malaria-infected erythrocyte separation. Lab Chip **10**(19), 2605–2613 (2010)
7. Harting, J., Harvey, M., Chin, J., Venturoli, M., Coveney, P.V.: Large-scale lattice Boltzmann simulations of complex fluids: advances through the advent of computational grids. Phil. Trans. R. Soc. Lond. A **363**, 1895–1915 (2005)
8. Binks, B.: Particles as surfactants–similarities and differences. Cur. Opin. Colloid Interface Sci. **7**(1–2), 21–41 (2002)
9. Frijters, S., Günther, F., Harting, J.: Effects of nanoparticles and surfactant on droplets in shear flow. Soft Matter **8**(24), 6542–6556 (2012)
10. Ramsden, W.: Separation of solids in the surface-layers of solutions and 'suspensions'. Proc. R. Soc. Lond. **72**, 156 (1903)
11. Pickering, S.: Emulsions. J. Chem. Soc. Trans. **91**, 2001–2021 (1907)
12. Stratford, K., Adhikari, R., Pagonabarraga, I., Desplat, J., Cates, M.: Colloidal jamming at interfaces: a route to fluid-bicontinuous gels. Science **309**(5744), 2198–2201 (2005)
13. Herzig, E., White, K., Schofield, A., Poon, W., Clegg, P.: Bicontinuous emulsions stabilized solely by colloidal particles. Nat. Mat. **6**(12), 966–971 (2007)
14. Succi, S.: The Lattice Boltzmann Equation. Oxford University Press, Oxford (2001)
15. Aidun, C., Clausen, J.: Lattice-Boltzmann method for complex flows. Ann. Rev. Fluid Mech. **42**, 439 (2010)
16. Shan, X., Chen, H.: Lattice Boltzmann model for simulating flows with multiple phases and components. Phys. Rev. E **47**, 1815 (1993)
17. Shan, X., Chen, H.: Simulation of nonideal gases and liquid-gas phase transitions by the lattice Boltzmann equation. Phys. Rev. E **49**, 2941 (1994)
18. Orlandini, E., Swift, M.R., Yeomans, J.M.: A lattice Boltzmann model of binary-fluid mixtures. Europhys. Lett. **32**, 463 (1995)
19. Dupin, M., Halliday, I., Care, C.: Multi-component lattice Boltzmann equation for mesoscale blood flow. J. Phys. A Math. Gen. **36**, 8517 (2003)
20. Peskin, C.: The immersed boundary method. Acta Numer. **11**, 479 (2002)
21. Kaoui, B., Krüger, T., Harting, J.: How does confinement affect the dynamics of viscous vesicles and red blood cells? Soft Matter **8**, 9246 (2012)
22. Jansen, F., Harting, J.: From bijels to Pickering emulsions: a lattice Boltzmann study. Phys. Rev. E **83**(4), 046707 (2011)
23. Günther, F., Janoschek, F., Frijters, S., Harting, J.: Lattice Boltzmann simulations of anisotropic particles at liquid interfaces. Comput. Fluids **80**, 184 (2013)
24. Günther, F., Frijters, S., Harting, J.: Timescales of emulsion formation caused by anisotropic particles. Soft Matter **10**, 4977 (2014)
25. Bleibel, J., Domínguez, A., Günther, F., Harting, J., Oettel, M.: Hydrodynamic interactions induce anomalous diffusion under partial confinement. Soft Matter **10**, 2945 (2014)
26. Kim, E., Stratford, K., Cates, M.: Bijels containing magnetic particles: a simulation study. Langmuir **26**(11), 7928 (2010)
27. Joshi, A., Sun, Y.: Multiphase lattice Boltzmann method for particle suspensions. Phys. Rev. E **79**, 066703 (2009)
28. Ladd, A., Verberg, R.: Lattice-Boltzmann simulations of particle-fluid suspensions. J. Stat. Phys. **104**, 1191 (2001)
29. Groen, D., Henrich, O., Janoschek, F., Coveney, P., Harting, J.: Lattice-Boltzmann methods in fluid dynamics: Turbulence and complex colloidal fluids. In: Bernd Mohr, W.F. (ed.) Jülich Blue Gene/P Extreme Scaling Workshop 2011. Jülich Supercomputing Centre, 52425 Jülich, Apr 2011. FZJ-JSC-IB-2011-02, http://www2.fz-juelich.de/jsc/docs/autoren2011/mohr1/

30. Schmieschek, S., Narváez Salazar, A., Harting, J.: Multi relaxation time lattice Boltzmann simulations of multiple component fluid flows in porous media. In: Nagel, M.R.W., Kröner, D. (eds.) High Performance Computing in Science and Engineering'12, p. 39. Springer, Heidelberg (2013)
31. Geislinger, T., Eggart, B., Braunmüller, S., Schmid, L., Franke, T.: Separation of blood cells using hydrodynamic lift. Appl. Phys. Lett. **100**, 183701 (2012)
32. Krüger, T., Varnik, F., Raabe, D.: Efficient and accurate simulations of deformable particles immersed in a fluid using a combined immersed boundary lattice Boltzmann finite element method. Comput. Math. Appl. **61**, 3485 (2011)
33. Krüger, T., Varnik, F., Raabe, D.: Particle stress in suspensions of soft objects. Phil. Trans. R. Soc. Lond. A **369**, 2414 (2011)
34. Krüger, T., Kaoui, B., Harting, J.: Interplay of inertia and deformability on rheological properties of a suspension of capsules. J. Fluid Mech. **751**, 725 (2014)
35. Ghosh, A., Harting, J., van Hecke, M., Siemens, A., Kaoui, B., Koning, V., Langner, K., Niessen, I., Rojas, J.P., Stoyanov, S., Dijkstra, M.: Structuring with anisotropic colloids. In: Proceedings of the Workshop Physics with Industry, Leiden, 17–21 Oct 2011. Stichting FOM (2011)
36. Wagner, A., Pagonabarraga, I.: Lees-Edwards boundary conditions for lattice Boltzmann. J. Stat. Phys. **107**, 521 (2002)